HHS Public Access

Author manuscript

Neuroscience. Author manuscript; available in PMC 2016 January 29.

Published in final edited form as:

Neuroscience. 2015 January 29; 285: 215–226. doi:10.1016/j.neuroscience.2014.10.035.

Caveolin expression changes in the neurovascular unit after juvenile traumatic brain injury: signs of blood-brain barrier healing?

Jérôme Badaut[1,2,3,*], **David O Ajao**[2], **Dane W Sorensen**[2,3], **Andrew M Fukuda**[2], and **Luc Pellerin**[4]

[1]CNRS UMR5287, University of Bordeaux, Bordeaux, France [2]Department of Physiology, Loma Linda University, Loma Linda, CA, USA [3]Department of Pediatrics, Loma Linda University, Loma Linda, CA, USA [4]Department of Physiology, University of Lausanne, Lausanne, Switzerland

Abstract

Traumatic brain injury (TBI) is one of the major causes of death and disability in pediatrics, and results in a complex cascade of events including the disruption of the blood-brain barrier (BBB). A controlled-cortical impact on post-natal 17 day-old rats induced BBB disruption by IgG extravasation from 1 to 3 days after injury and returned to normal at day 7. In parallel, we characterized the expression of three caveolin isoforms, cav-1, cav-2 and cav-3. While cav-1 and cav-2 are expressed on endothelial cells, both cav-1 and cav-3 were found to be present on reactive astrocytes, *in vivo* and *in vitro*. Following TBI, cav-1 expression was increased in blood vessels at 1 and 7 days in the perilesional cortex. An increase of vascular cav-2 expression was observed 7 days after TBI. In contrast, astrocytic cav-3 expression decreased 3 and 7 days after TBI. Activation of eNOS (via its phosphorylation) was detected 1 day after TBI and phospho-eNOS was detected both in association with blood vessels and with astrocytes. The molecular changes involving caveolins occurring in endothelial cells following juvenile-TBI might participate, independently of eNOS activation, to a mechanism of BBB repair while, they might subserve other undefined roles in astrocytes.

Keywords

blood-brain barrier; endothelium; astrocyte; juvenile traumatic brain injury; caveolin

[*]**Corresponding Author**: Jérôme Badaut, PhD, University of Bordeaux, CNRS UMR 5287, 146 rue Leo Saignat, 33076 Bordeaux cedex, France, Jerome.badaut@u-bordeaux.fr, Phone: +33 5 57 57 17 35, Fax : +33 5 56 90 14 21.

Author's contributions:

DA, AF, DS, and JB: generated the data; experimental design and the analysis, JB, writing JB and LP

Disclosure/Conflict of Interest

The authors declare no conflict of interest

INTRODUCTION

Traumatic brain injury (TBI) affects about 1.7 million persons annually and accounts for about 30.5% of all injury-related deaths in the United States. Children and adolescents aged between 0 and 14 years represent a vulnerable population with half a million TBI-related emergency department visits annually (Faul et al., 2010). As such, juvenile TBI (jTBI) is a leading cause of death and disability in children and adolescents in the United States (Schneier et al., 2006). TBI is defined as brain damage that results from an external mechanical force (e.g. rapid acceleration or deceleration), blast waves, penetration by a projectile, or direct impact, and it is often accompanied by a post-injury concussion or similar forms of altered consciousness. In connection with the primary injury, jTBI is associated with secondary events, which include hemorrhage, disruption of the blood-brain barrier (BBB), and vasogenic edema (Pop and Badaut, 2011). TBI in the juvenile population has been associated with greater risks of cerebral hemodynamic dysfunction, hypoxic-ischemic injury, and diffuse cerebral edema compared to adults (Giza et al., 2007). In an experimental model of jTBI, we have previously shown an increase in brain water content during the first week post-injury using T2-weighted MRI (Fukuda et al., 2012). TBI-induced vascular changes have been shown to alter endothelial phenotypes both acutely and chronically after injury (Pop and Badaut, 2011, Pop et al., 2013). Interestingly, recent studies have associated caveolin-1 (cav-1) with BBB dysfunctions in several brain injury models (Jasmin et al., 2007, Nag et al., 2007, Nag et al., 2009, Gu et al., 2011). However, controversial reports have been published on the role of cav-1 in acute BBB dysfunctions after brain injuries: a beneficial role of increased cav-1 by inhibition of NO synthesis (Gu et al., 2011) or a deleterious role with harmful effects on the BBB (Nag et al., 2007, Nag et al., 2009, Chang et al., 2011).

Caveolins are structural proteins involved in the formation of caveolae, which are known to be involved in endocytosis, transcytosis, and exocytosis in endothelial cells (Predescu et al., 2007). Three caveolin isoforms are known to be expressed in the mammalian brain (Cameron et al., 1997, Virgintino et al., 2002). Cav-1 and caveolin-2 (cav-2) have been mostly found in brain endothelial cells (Virgintino et al., 2002) although cav-1 has also been observed in some neurons and astrocytes (Cameron et al., 1997, Virgintino et al., 2002). Brain caveolin-3 (cav-3) has been predominantly described in astrocytes (Virgintino et al., 2002, Shin et al., 2005). Besides facilitating the caveolae sequestration of several receptors, transporters and ligands, caveolins also serve as active modulators of activities of a wide variety of signaling molecules, and in particular by inhibiting the endothelial nitric oxide synthase (eNOS) (Bucci et al., 2000, Lajoie et al., 2009).

Despite an abundant literature on the role of cav-1 in modulating eNOS and its physiological consequences in the periphery (Bernatchez et al., 2005), in comparison little is known about the potential roles of caveolins after brain injury. In several models of adult brain injuries, the level of expression of cav-1 is increased in the endothelium for several days following cold cortical injury (Nag et al., 2007, Nag et al., 2009), brain ischemia(Jasmin et al., 2007) and experimental spinal cord injury(Shin et al., 2005, Shin, 2007). Although cav-1 increase in some of these brain injury models was associated with BBB or blood-spinal cord barrier breakdown (Nag et al., 2007, Nag et al., 2009), the exact role of these changes in cav-1 is

still unclear. Experiments using cav-1 knockout (cav-$1^{-/-}$) mice suggest beneficial roles for cav-1 in rodent models of brain disorders (Jasmin et al., 2007, Gu et al., 2011). In fact, cav-$1^{-/-}$ mice presented higher vascular permeability (Schubert et al., 2002, Siddiqui et al., 2011) and intriguingly have a worse outcome than the wild-type (WT) with increased cerebral volume of infarction after stroke (Jasmin et al., 2007). Interestingly, claudin-5, a protein involved in tight junction (TJ) formation and p-glycoprotein (P-gp), an ATP-binding protein, were shown to bind to cav-1 and be stabilized by it (McCaffrey et al., 2007, Stamatovic et al., 2009, McCaffrey et al., 2012). It is therefore plausible that increase in cav-1 expression may be contributing to the recovery of TJ and BBB functions after injury.

Apart from cav-1, cav-2 was also shown to be abundant in endothelial cells, and cav-$2^{-/-}$ mice showed a decreased lesion volume compared to WT after stroke (Jasmin et al., 2007). This suggests that cav-2 may have a detrimental role in brain injury, in contrast with cav-1. Lastly, cav-3 expression was also shown to change in spinal cord astrocytes in a model of experimental autoimmune encephalomyelitis (Shin et al., 2005) and could also have a role to play in some cerebral pathologies.

The changes in expression of these caveolins are potentially contributing to the neurovascular dysfunctions observed after jTBI (Fukuda et al., 2012, Pop et al., 2013). The expression and distribution profiles of cav-1, -2, and -3 within the neurovascular unit after jTBI in conjunction with BBB dysfunction have not been investigated in association with the changes of eNOS activation. The goal of the present study was, therefore, to follow changes in the level of expression of cav-1, -2, and -3, in parallel with the changes in BBB functions and eNOS signaling during the first week after jTBI.

2. Material and Methods

2.1. Animals

Manuscript was written in accordance with the ARRIVE guidelines. All animal related protocols and procedures in this study were approved by the Institutional Animal Care and Use Committee of Loma Linda University. Male Sprague-Dawley rat pups at postnatal day 10 (P10, Harlan, Indianapolis, IN) were housed on a 12-hour light-dark cycle at constant temperature and humidity for one-week prior to surgery to allow sufficient time for acclimatization. Following induction of experimental brain injury or sham procedure at P17 (30± 4 g, n=66 rats), the pups were returned to their cages with their dams and subsequently weaned at 7d. They were housed two rats per cage, and fed with standard lab chow and water *ad libitum*. Identical sham or controlled cortical impact (CCI) surgical parameters were used for the experimental brain injury.

2.2. Juvenile Traumatic Brain Injury Model

Controlled cortical impact (CCI) was induced in P17 old rat pups as previously described (Ajao et al., 2012, Fukuda et al., 2012). Briefly, rat pups were anesthetized with isoflurane (Webster Veterinary Supply, Inc., Sterling, MA) and placed into a stereotaxic frame (David Kopf Instruments, USA). A 5 mm diameter craniotomy was drilled over the right parietal cortex at 3 mm anterior-posterior and 4 mm medial-lateral to bregma. CCI was induced in

the jTBI group using a 2.7mm diameter rounded-tip metal impactor fixed to an electromechanical actuator (Leica Microsystems Company, Richmond, IL) and centered over the exposed dura at a 20° angle to the cortical surface. The impact was delivered at a velocity of 6 m/s, with impact duration of 200 ms, and to a depth of 1.5 mm from the cortical surface. Bleeding and convexity of the injured cortex were recorded and showed no significant difference within the jTBI animals. The surgical site was sutured closed. Appropriate pain management was provided through subcutaneous administration of Buprenorphine (0.01 mg/kg; dilution: 0.01 mg/ml) immediately following end of suturing. The body temperature was maintained at 37°C throughout the surgical procedure. Sham animals underwent identical procedures with the exception of cortical impact. All rats recovered from anesthesia within 25 minutes post-injury. No seizures resulting from experimental procedure was observed within the 2 to 3-hour observation period immediately following injury when the animals were returned to their cages.

2.3. Astrocyte cultures

Primary cortical astrocyte-enriched cultures were prepared from mice at postnatal day 1 as previously described (Pellerin and Magistretti, 1994). Following isolation of cortices and removal of the meninges, dissociated cells were suspended in DMEM supplemented with 10% FCS and Antibiotic-Antimycotic. Cells were seeded on 24-well plates for growing period of 21 (±2) d at 37°C and 5% CO2. Medium was exchanged every 3–4 d. Cells were fixed with PFA 4% in PBS for 15min and then rinsed with PBS 3 times before to perform the immunohistochemistry.

2.4. Western Blotting

A set of rats was prepared with 5 to 7 animals per group at 1d, 3d and 7d brains were freshly dissected and the cortical tissue adjacent to the site of the impact was collected. Tissues were prepared in RIPA buffer with a cocktail of protease inhibitors (Roche, Basel, Switzerland) and sonicated for 30s. After BCA protein assay, 10 μg of protein was then subjected to SDS polyacrylamide gel electrophoresis on a 4–12% gel (Nupage, Invitrogen, Carlsbad, CA). Proteins were then transferred to a polyvinylidene fluoride membrane as indicated by the supplier (PerkinElmer, Germany). The blot was incubated with a rabbit polyclonal against cav-1 (BD Biosciences, 1:2000), pi-eNOS (cell signalling, 1:1000), and a monoclonal antibody against Tubulin (Sigma, USA, 1:10,000); a monoclonal antibody against cav-2 or cav-3 (BD Biosciences, 1:2000), claudin-5 (1:200, Life Technologies: Invitrogen, Grand Island, NY, USA), P-gP (1:100, EMD Chemicals, Merck KGaA, Darmstadt, Germany) and a polyclonal antibody against actin (Sigma, USA, 1:25,000) in Odyssey blocking buffer (LI-COR, Bioscience, Germany) overnight at 4°C. After washing, the blot was incubated with two fluorescence-coupled secondary antibodies (1:10,000, anti-rabbit Alexa-Fluor-680nm, Molecular Probes, Oregon and anti-mouse IR-Dye-800-nm, Roche, Germany) for 2 hours at room temperature. After washing, the degree of fluorescence was measured using an infra-red scanner (Odyssey, LI-COR, Germany).

2.6. Tissue Processing and Immunohistochemistry

A second set of rats were transcardially perfused with 4% PFA prepared in PBS at 1d, 3d, and 7d with n=5 rats per group (jTBI and sham) for each time points. The brains were

removed and immersed in 30% sucrose at 4°C for 48 hours and then frozen on dry ice and stored at −20°C pending tissue cutting. Coronal cryostat sections (Leica CM1850, Leica Microsystems GmbH, Wetzlar, Germany) were prepared.

2.3.1. IgG extravasation staining for BBB assessment—To evaluate the BBB disruption, IgG extravasation staining was performed as previously described (Badaut et al., 2011). Briefly, the sections were incubated with biotin conjugated affinity purified goat anti-rat IgG coupled with Infrared-Dye-800-nm (1:500 dilution; Rockland, Gilbertsville, PA) in PBS containing 0.1% Triton X-100 and 1% bovine serum albumin (BSA) for 2 hours at room temperature. After washing, sections were dried and scanned on an infra-red scanner (Odyssey-system, LiCor, Germany) to quantify the area of the IgG extravasation for three adjacent slices covering the lesion with the LI-COR Odyssey system.

2.3.2. Double immunohistochemistry analysis—All antibody incubations were carried out in PBS (Fisher Scientific, Pittsburgh, PA) containing 0.25% Triton X-100 and 0.25% BSA (both from Sigma-Aldrich Co., St. Louis, MO). After washes in PBS, sections were blocked for 1.5 hours in PBS with 1% BSA, and then incubated overnight at 4°C with one of the following: mouse anti-cav-1 or -2 or -3 (each diluted 1:200; BD Biosciences, San Jose, CA), rabbit anti-cav-1 (1:200; Abcam Inc., Cambridge, MA), mouse anti-claudin-5 (1:100; Invitrogen, Camarillo, CA), mouse anti-P-gP (1:100, EMD Chemicals, Merck KGaA, Darmstadt, Germany), mouse anti-NeuN (1:500; Abcam Inc., Cambridge, MA), rabbit polyclonal antibodies for IBA-1 (1:300; Wako), and chicken anti-glial fibrillary acidic protein (GFAP, 1:1000; Millipore, Billerica, MA). After 3×10min PBS rinses, sections were incubated for 2 hours at room temperature with a mixture of goat anti-mouse secondary antibody coupled with Alexa-Fluor-488 and goat anti-rabbit secondary antibody coupled with Alexa-Fluor-568 (both at 1:1000; Invitrogen, Camarillo, CA) and subsequently rinsed again in PBS for 3×10 minutes. Sections stained with the antibodies mentioned were all mounted on glass slides and coverslipped with anti-fading medium vectashield containing DAPI (Vector, Vector Laboratories, Burlingame, CA).

Negative control staining where the primary antibody was omitted showed no detectable labelling.

The area of cav-1 and cav-2 immunolabeling was quantified at 1, 3, 7, and 60d from a series of images collected at 20× objective (422 μm × 338 μm) in perilesional parietal cortex and ipsilateral temporal cortex using an epifluorescent microscope with the same parameters for all animals (Olympus, BX41, Center Valley, PA). Images were acquired from five serial coronal slices separated by 500 μm (24 images per animal). The area of cav-1 and cav-2 staining was measured for each individual image with MorphoPro software (Explora-Nova, La Rochelle, France) according to the following procedure: 1) Top Hat morphologic filter to outline vascular staining from the background, 2) user-defined threshold value applied to each image. Final values were represented as a percentage of the sham group.

2.7. Statistical analyses

All data are presented as mean ± SEM, statistical analyses were done using SPSS, and graphs obtained using SigmaPlot. The IgG extravasation, cav-1, cav-2 immunolabeling, and

western blot data were analyzed using student t-tests for normally distributed data with comparison between the sham and jTBI groups for each individual time points.

3. RESULTS

3.1. Blood-Brain Barrier disruption in early time-points after jTBI

Changes in BBB integrity were assessed at various time-points following jTBI. In order to evaluate BBB disruption from 1d to 7d on the same group of rats, we used the IgG extravasation staining (Fig. 1A–C). Increased staining of extravasated IgG was observed in the perilesional area and contralateral cortex of jTBI animals (Fig. 1B, C) at 1d and 3d compared to the sham group. The IgG staining decreased back to normal (i.e. sham) level at 7d (Fig. 1B, C). Quantification of extravasated IgG showed a significant increase in the perilesional cortex of jTBI rats at 1d and 3d compared to sham (respectively 0.023 ± 0.033 mm^2 vs 0.002 ± 0.001 A.U and 0.035 ± 0.042 A.U vs 0.002 ± 0.001 A.U, $p<0.05$, Fig. 1C). This suggests that BBB disruption is maximum at 1d and 3d post-injury, which is in agreement with our previous observations that showed vasogenic edema formation between 1d and 3d, followed by normalization after 7d (Fukuda et al., 2012).

To further characterize the changes in BBB properties, we carried out western blot and immunohistochemical analyses for two key proteins for BBB function, a protein of the tight junctions, claudin 5 and for an ATP binding transporter, P-gp in accordance with our previous work (Pop et al., 2013). Interestingly, western blot analysis of the level of expression of claudin-5 exhibited a bi-phasic variation characterized by a 21% decrease of claudin-5 expression in the jTBI group compared to the sham at 3d ($p<0.05$, Fig. 1D). Such a decrease in claudin-5 expression corresponds to the peak of BBB disruption (Fig. 1B, C). On the other hand, the normalization of IgG extravasation is associated with a significant increase of the claudin-5 expression of 39% in jTBI group compared to the sham by 7d (Fig. 1D). Correspondingly, Claudin-5 IR associated with blood vessels exhibited a decrease at 3d in the ipsilateral cortex in the jTBI group compared to the sham group (Fig. 1E2,F2). At 7d, claudin-5-IR found on blood vessels was increased compared to the sham level (Fig. 1E3,F3), suggesting a compensatory mechanism as we previously described at 60 days post jTBI (Pop et al., 2013). P-gp expression analysis by western blot, revealed a 37% increase ($p<0.05$) in jTBI group compared to the sham at 7d (Fig. 1G). The immunohistochemistry staining illustrated that the significant increase of P-gP staining at 7d (Fig 1I) compared to the sham (Fig 1I) occurs in the blood vessels outlined with tomato-lectin staining (t-lectin).

3.2.Changes in expression of caveolin-1, -2, and -3 within the neurovascular unit after jTBI

3.2.1 Immunocytochemical localization of the three caveolins in the cortex after jTBI—In order to determine the cellular localization of cav-1, various cav-1 antibodies were used in double immunostaining with other cell markers to identify the cell distribution of cav-1 after jTBI in the tissue adjacent to the lesion and remotely. As previously described, anti-cav-1 staining showed that cav-1 is predominantly expressed in brain endothelial cells (Fig. 2A, B) of all cerebral blood vessels, independent of the diameter (from the pial vessels to intracerebral arterioles and capillaries) in normal brain (not shown) and at distance from the site of the injury. In parallel, cav-2-IR was observed in brain

endothelial cells in brain blood vessels of all sizes including pial blood vessels in both sham and jTBI groups (Fig. 2C). Double immunolabeling for cav-1 and cav-2 showed the co-localization of the two proteins in the endothelium of cerebral blood vessels, suggesting that cav-1 and cav-2 could bind together (Fig 2D1–3). Double immunolabeling for GFAP and cav-1 showed co-localization, suggesting the presence of cav-1 in reactive astrocytes at the border of the lesion at 1d and 3d following jTBI (Fig. 2E1–3). Anti-cav-1 staining also co-localized with mouse anti-NeuN staining (Fig. 3A), suggesting an increased immunoreactivity of cav-1 in neurons located around the lesion site at 3d post-injury. However, cav-1 staining did not co-localize with IBA-1 staining, a marker of microglial cells (Fig. 3B). Cav-3 immunostaining was observed in astrocytes located in the glia limitans, cortex, hippocampus, white matter tract and hypothalamus in both groups (data not shown). Double immunolabeling of GFAP and cav-3 confirmed the presence of cav-3 in astrocytes (Fig. 2F). A positive immunostaining for cav-1 was observed in primary astrocyte cultures, confirming its presence in reactive astrocytes (Fig. 2G). Similarly, positive cav-3 IR was observed in the primary astrocyte cultures (Fig. 2H).

3.2.2 Time-dependent changes in caveolin-1 expression following jTBI—The relative changes of cav-1-IR in the ipsilateral cortical tissue, including the cavity at 1d, 3d and 7d following jTBI were quantified by western blot. A specific band was observed at 22 kDa, and the changes of cav-1 expression showed a bi-phasic profile (Fig. 4A) during the first week after the injury. The level of expression of cav-1 was significantly increased in jTBI compared to sham at 1d and 7d (Fig. 4A, B; $p<0.05$). At 3d, the level of expression of cav-1 was slightly decreased compared to the sham. The immunohistochemical labeling for cav-1 showed a similar pattern in the endothelium, with an increase in the staining of brain cortical blood vessels from 1d and 7d (Fig. 4D1, D2) in the perilesional area compared to the sham groups (Fig. 4C1, C2). In fact, the immunofluorescence quantification showed that cav-1-IR in cerebral blood vessels in the ispilateral cortex is significantly increased by 36% at 1d and 92% at 7d compared to the sham groups ($p<0.05$).

3.2.3 Time-dependent changes in caveolin-2 expression following jTBI—The relative changes of cav-2-IR in the ipsilateral cortical tissue at 1d, 3d and 7d following jTBI were quantified by western blot. The western blot showed a band around 24 kDa in both sham and jTBI (Fig. 5A). Interestingly, the level of expression of cav-2 showed a similar pattern of changes than cav-1, with an increase of its expression at 1d and a significantly higher at 7d in jTBI animals compared to the sham group. However, there is no difference at 3d, with the same level of expression between sham and jTBI (Fig. 5A). The analysis of the level of cav-2 immunofluorescence was performed on the same regions of interest that was used for cav-1. As observed with the western blot analysis, cav-2 immunofluorescence is significantly increased by 95 % in cortical blood vessels in jTBI group compared to sham at 7d post-injury (Fig. 5B, C).

3.2.4 Time-dependent changes in caveolin-3 expression following jTBI—The relative changes of cav-3-IR in the ipsilateral cortical tissue at 1d, 3d and 7d following jTBI were quantified by western blot. Western blot of cav-3 showed a band around 20kDa (Fig 6A). A significant decreased of cav-3 expression at 3d and 7d in jTBI groups was observed

compared to the sham groups (Fig. 6A, B). Immunohistochemical analysis of cav-3 showed changes in the pattern of the staining. First, the presence of cav-3 in glia limitans is not observed in jTBI animals at 3 and 7d post-injury (Fig. 6D2, 6D3) compared to sham animals (Fig. 6C2, 6C3). Surface area of cav-3 staining is also more extended in the astrocytes in the vicinity of the cortical lesion (Fig. 6D2, 6D3) compared to the sham group (Fig. 6C2, 6C3), an effect that is likely due to the changes of the properties of the astrocytes after jTBI. Overall the intensity of cav-3 immunofluorescence at 3 and 7d post-jTBI (Fig. 6D2, 6D3) seems to be decreased compared to the sham group (Fig. 6C2, 6C3).

3.3. Changes in eNOS signaling in early time-points after jTBI

As indicated in the introduction, caveolin is known to bind to eNOS and to regulate its activation. We addressed the question of eNOS activation under our conditions by measuring the level of phospho-eNOS (pi-eNOS) by western blot. Total eNOS expression was not different between the groups, while pieNOS appearing as an expected band at 140 kDa, exhibited changes between the groups. The level of expression of pi-eNOS in the jTBI group is augmented by 49% compared to sham at 1d (Fig. 7A). In a second phase, the expression of pi-eNOS is significantly decreased in the jTBI group compared to sham by 22% at 3d (Fig. 7A). There was no difference at 7d after brain injury. Immunohistochemical labelings showed that the expression of pi-eNOS is present in the endothelium (Fig. 7B) of blood vessels outlined by tomato-lectin staining (Fig. 7C). Surprisingly, a large part of the expression of pi-eNOS was associated with the astrocytes suggesting that the global changes of pi-eNOS expression observed in the perilesional cortex might also be due to astrocytic expression. The presence of pi-eNOS in astrocytes was confirmed by a positive immunolabeling in primary astrocyte cultures (Fig 7D) co-localizing both *in vitro* and *in vivo* after jTBI with cav-3 in astrocytes (Fig. 7D,E) and cav-1 (data not shown). Cav-1 and pi-eNOS also co-localized in the endothelium of blood vessels in addition to astrocytes (Fig. 7F), suggesting potential interactions between the molecular pathways.

4. DISCUSSION

Traumatic brain injury in the juvenile population is known to be associated with greater risks of cerebral hemodynamic dysfunction, BBB disruption, and diffuse cerebral edema, compared to adults (Armstead, 1999, Campbell et al., 2007, Giza et al., 2007). BBB disruption in clinical patients is known to be a major cause of mortality and long-term neurological deficits in victims with moderate to severe TBI (Shlosberg et al., 2010). There is also more evidence indicating that in mild TBI such as in blast injury, the BBB is impaired early on after the injury (Readnower et al., 2010). Hence, there is a need to study BBB changes in jTBI after injury as well as the molecular processes involved in BBB repair. The jTBI model showed a significant increase in IgG extravasation with a peak at 3d, paralleled with the loss of claudin-5 staining in the cortex, and these findings indicate a physical BBB disruption during the development of secondary injuries. It is interesting to note that BBB disruption parallels the peak of edema formation previously observed on the T2-weighted MRI in a similar jTBI model (Fukuda et al., 2012). At 7d, the extravasation of IgG returned to sham levels when claudin-5 expression is increased, suggesting a recovery of BBB tight junctions. Similarly, BBB recovery parallels the increase of P-gp and the

decrease in vasogenic edema previously observed as a return to the normal T2 values on T2-weighted MRI scans at 7d in a similar injury model (Fukuda et al., 2012). It is interesting to outline that the increase of claudin-5 expression observed at 7d is still present 2 months post-jTBI (Pop et al., 2013), which is part of the long-term phenotypic changes at the endothelium.

Increase of cav-1 and cav-2 expression in endothelial cells predicts BBB recovery

Endothelial cav-1 and cav-2 proteins could be good molecular candidates to study with regard to changes in BBB properties because of their possible involvement in the regulation of several intracellular signaling processes (Bucci et al., 2000, Gu et al., 2011). In fact, cav-1 was shown to be involved in the regulation of eNOS activity (Bucci et al., 2000, Bernatchez et al., 2005), as well as in the stabilization of tight junction proteins such as claudin-5 within the lipid raft domain and of P-gp (Jodoin et al., 2003, McCaffrey et al., 2007, McCaffrey et al., 2012). Enhancement of cav-1 expression was proposed to be beneficial in cerebral ischemia model by limiting the increase of activation of eNOS, and NO production with for consequences a limited activation of matrix metalloproteinases (MMPs) and reduced degradation of the perivascular extracellular matrix (Gu et al., 2011).

After jTBI, cav-1 but also cav-2 expression is slightly increased at 1d, before to go back to the value observed in sham groups. However, the increase of both caveolins seems to have no effect to limit the activation of eNOS, represented by a significant increase of pi-eNOS. This result strongly suggests that in jTBI an increase of NO production occurs, unabated by enhanced caveolin expression, with a toxic effect on the BBB properties. At the peak of the BBB disruption (measured with IgG extravasation), claudin-5 was significantly decreased when cav-1 and cav-2 protein expression in jTBI rats showed values similar to shams. At this time point pi-eNOS is decreased, further showing that eNOS activation seems independent of caveolin expression levels.

The profile of cav-1 and 2 expression in the endothelial cells after jTBI shares some similarities with previous findings in other adult rodent models of CNS insults. In fact, an early increase of cav-1 in the endothelial cells preceded the decrease of claudin-5 and occludin (Nag et al., 2007, Nag et al., 2009). From this study, the authors concluded that the increase of cav-1 expression could potentially contribute to BBB disruption by inducing transcytosis of proteins across the cerebral endothelium (Nag et al., 2007, Nag et al., 2009). In contrast, cav-1 could exhibit some effects rather promoting BBB integrity. Thus, tight junction proteins such as claudin-5 and occludin have been shown to bind to and be stabilized by cav-1 within the caveolae (McCaffrey et al., 2007). After hypoxia-reoxygenation, levels of claudin-5 and occludin found within the caveolae were all together reduced (McCaffrey et al., 2007, McCaffrey et al., 2009). From this work, cav-1 was rather proposed to play a beneficial role in the maintenance of these tight junction protein subunits (McCaffrey et al., 2007, McCaffrey et al., 2009, Stamatovic et al., 2009). Moreover, cav-1$^{-/-}$ mice presented higher endothelial permeability in the systemic vasculature compared to WT (Razani et al., 2001, Schubert et al., 2002). Therefore, a decrease in cav-1 expression may suggest a disruption in the BBB integrity (as observed from 1d to 3d after jTBI following the initial increase), whereas an increase of cav-1, as observed at 7d, may be

beneficial toward the recovery of the BBB integrity after jTBI. In support of this hypothesis, cav-$1^{-/-}$ mice showed a larger lesion volume compared to WT in a transient middle cerebral artery occlusion model (Jasmin et al., 2007). The beneficial role of cav-1 could involve different mechanisms: 1) cav-1 seems essential to promote angiogenesis as its absence is detrimental due to a decrease in angiogenesis in cav-$1^{-/-}$ mice compared to WT (Jasmin et al., 2007); 2) since cav-1 has a caveolin scaffolding domain that binds to eNOS and inhibits its activity (Bucci et al., 2000), it could prevent the toxic effects of NO (Gu et al., 2011). Indeed, a decrease of NO formation following an increase of cav-1 expression in a stroke model has been shown to be associated with decreased activation of MMPs (Gu et al., 2011) and consequently to a protection of the BBB. Therefore, the experiments with cav$1^{-/-}$ suggest that an increase of cav-1 expression in the endothelium at 7d following jTBI may be an endogenous mechanism aimed at facilitating BBB recovery during the first week. However, considering the time course of the changes observed with the different proteins, the parallel changes of cav-1 and cav-2 expression and the improvement of the BBB strongly suggest that an increased expression of these proteins may stabilize other BBB proteins like claudin-5 and P-gP, rather than to play directly on the NO pathway as it was proposed in stroke (Gu et al., 2011). So far, the exact role of cav-1 in brain injury and especially in jTBI remains unknown, and detrimental effects of acute cav-1 increase cannot be ruled out. In fact, an increase in cav-1 and cav-2 staining could be associated with an increase in the number of caveolae, which in turn is responsible for increased transcytosis (Jodoin et al., 2003, Regina et al., 2004) and the entrance of albumin, which may contribute to the dysfunction of the brain tissue homeostasis (Komarova and Malik, 2010). Indeed, such an effect could be associated with the early increase in cav-1 after 1 day and participate to the early BBB disruption as previously proposed (Nag et al., 2007, Nag et al., 2009).

Cav-1 and cav-3 expression in astrocytes: negative role in astrogliosis?

In the juvenile rat brain, the main cav-1 and cav-2 expression is associated with the endothelial cell layer of cerebral blood vessels of all sizes (from capillaries to pial arteries) in accordance with previous studies carried out in adult mammalian brains (Cameron et al., 1997, Virgintino et al., 2002). However, the expression of the caveolins was not limited to the endothelial cells. Cav-1 was also found in some parenchymal cells such as astrocytes and neurons in the jTBI group, a finding also reported in previous studies (Ikezu et al., 1998, Virgintino et al., 2002, Head et al., 2008). The presence of cav-1 in astrocytes, which co-localizes with GFAP staining *in vivo* as reported before (Ikezu et al., 1998), was confirmed in primary astrocyte cultures like observed in previous work (Wiencken and Casagrande, 1999).

In addition to cav-1, reactive astrocytes after jTBI exhibited the presence of cav-3 staining. Indeed, cav-3 co-localized with GFAP staining *in vivo*, which is consistent with previous studies in adult models (Ikezu et al., 1998, Shin et al., 2005) and confirmed in the primary astrocyte cultures. Although cav-3 has been reported in smooth muscles (Ikezu et al., 1998), we did not observe any cav-3 staining in intraparenchymal cerebral blood vessels. The expression and localization of cav-3 in jTBI brains appear to coincide with astrogliosis, which is similar to findings in experimental autoimmune encephalomyelitis (Shin et al., 2005). However, the level of expression of cav-3 is significantly decreased at 3 and 7 days

post-injury. Associated with this decrease of the protein level, the pattern of cav-3 staining changed with a weaker signal in astrocyte processes in jTBI compared to shams. A possibility is that the decrease of cav-3 could be compensated by the increase of cav-1 expression in reactive astrocytes, which was mostly detected with a rabbit polyclonal anti-cav-1 as previously described (Virgintino et al., 2002, Shin et al., 2005). The exact roles of these proteins in astrocytes *in vivo* are still unknown. Caveolins can be associated with eNOS, which was previously shown to be present in astrocytes of the rat brain (Colasanti et al., 1998, Wiencken and Casagrande, 1999). In our experiments, we observed the presence of pi-eNOS in astrocytes both *in vitro* and *in vivo*. Moreover, both cav-3 and cav-1 present in astrocytes co-localized with pi-eNOS after jTBI. In astrocytic culture, cav-1 was observed to function as an endogenous inhibitor of eNOS activation (Colasanti et al., 1998). However, the changes in pi-eNOS expression are independent of cav-1 and cav-3 expression, thus questioning a role of caveolins in a putative inhibition of eNOS activation and excess release of NO following jTBI. Interestingly, the changes of the level of expression of cav-1 in astrocyte cultures were associated with opposite changes in expression of the glutamate transporter GLT1 (Zschocke et al., 2005, Gonzalez et al., 2007). The application of transforming growth factor-alpha (TGF-α) induced a decrease of cav-1 and an increase of GLT1 (Zschocke et al., 2005, Gonzalez et al., 2007). Increase of cav-1 expression in the astrocyte may, therefore, participate to the mechanism producing a downregulation of GLT1 in the astroglia. Such a reduced GLT1 expression could have important consequences on glutamate uptake and excitotoxicity after jTBI. Additional experiments will be needed to determine the functional roles of these 2 caveolins in astrocytes.

Summary

Cav-1 and cav-2 expression profile after jTBI parallels the resolution of the BBB disruption using claudin-5 and P-gp expression as markers. In contrast with adult brain injury, the changes in cav-1 and cav-2 expression are not directly related to the inhibition of eNOS activation revealed indirectly with the level of expression of pi-eNOS. These observations suggest that the molecular mechanisms involved in BBB dysfunctions could differ depending of the cause of the insult as well as the age at which it occurs. Moreover, each cell constituting the NVU (i.e. endothelial cell, neuron, astrocyte) has to be considered, especially with the finding of the presence of cav-1 and cav-3 in astrocytes. This study shows for the first time changes in the expression of these molecules in a model of jTBI and the complexity of the role of the caveolins. Further studies will be needed to characterize the role of each caveolin in each cell type after jTBI.

Acknowledgements

The authors thank Dr. Viorela Pop, Nina Nishiyama and Germaine Paris for her help for part of the histology and tissue analysis. They are also grateful to Cendrine Repond for preparing the primary cultures of mouse cortical astrocytes.

A portion of this material was performed in the Loma Linda University School of Medicine Advanced Imaging and Microscopy Core that is supported by the National Science Foundation under Major Research Instrumentation, Division of Biological Infrastructure Grant No. 0923559 (Dr Sean M Wilson) and the Loma Linda University School of Medicine.

Grant information: This work was supported in part by NINDS grant R01HD061946 (JB) and the Loma Linda University Department of Pediatrics Research Fund, and the Swiss Science Foundation (FN 31003A-122166, JB) at Loma Linda University.

LIST OF ABBREVIATIONS

jTBI	juvenile traumatic brain injury
TBI	traumatic brain injury
BBB	blood brain barrier
Cav-1	caveolin 1
Cav-2	caveolin 2
Cav-3	caveolin 3
CSD	caveolin scaffolding domain
d	days post injury
CCI	controlled cortical impact

REFERENCES

Ajao DO, Pop V, Kamper JE, Adami A, Rudobeck E, Huang L, Vlkolinsky R, Hartman RE, Ashwal S, Obenaus A, Badaut J. Traumatic brain injury in young rats leads to progressive behavioral deficits coincident with altered tissue properties in adulthood. J Neurotrauma. 2012; 29:2060–2074. [PubMed: 22697253]

Armstead WM. Cerebral hemodynamics after traumatic brain injury of immature brain. Exp Toxicol Pathol. 1999; 51:137–142. [PubMed: 10192582]

Badaut J, Ashwal S, Adami A, Tone B, Recker R, Spagnoli D, Ternon B, Obenaus A. Brain water mobility decreases after astrocytic aquaporin-4 inhibition using RNA interference. J Cereb Blood Flow Metab. 2011; 31:819–831. [PubMed: 20877385]

Bernatchez PN, Bauer PM, Yu J, Prendergast JS, He P, Sessa WC. Dissecting the molecular control of endothelial NO synthase by caveolin-1 using cell-permeable peptides. Proc Natl Acad Sci U S A. 2005; 102:761–766. [PubMed: 15637154]

Bucci M, Gratton JP, Rudic RD, Acevedo L, Roviezzo F, Cirino G, Sessa WC. In vivo delivery of the caveolin-1 scaffolding domain inhibits nitric oxide synthesis and reduces inflammation. Nat Med. 2000; 6:1362–1367. [PubMed: 11100121]

Cameron PL, Ruffin JW, Bollag R, Rasmussen H, Cameron RS. Identification of caveolin and caveolin-related proteins in the brain. J Neurosci. 1997; 17:9520–9535. [PubMed: 9391007]

Campbell SJ, Carare-Nnadi RO, Losey PH, Anthony DC. Loss of the atypical inflammatory response in juvenile and aged rats. Neuropathol Appl Neurobiol. 2007; 33:108–120. [PubMed: 17239013]

Chang CF, Chen SF, Lee TS, Lee HF, Chen SF, Shyue SK. Caveolin-1 deletion reduces early brain injury after experimental intracerebral hemorrhage. Am J Pathol. 2011; 178:1749–1761. [PubMed: 21435456]

Colasanti M, Persichini T, Fabrizi C, Cavalieri E, Venturini G, Ascenzi P, Lauro GM, Suzuki H. Expression of a NOS-III-like protein in human astroglial cell culture. Biochem Biophys Res Commun. 1998; 252:552–555. [PubMed: 9837744]

Faul, M.; Xu, L.; Wald, MM.; Coronado, V. National Center for Injury Prevention and Control. Atlanta, GA: CDC; 2010. Traumatic brain injury in the United States: emergency department visits, hospitalizations, and deaths, 2002–2006.

Fukuda AM, Pop V, Spagnoli D, Ashwal S, Obenaus A, Badaut J. Delayed increase of astrocytic aquaporin 4 after juvenile traumatic brain injury: Possible role in edema resolution? Neuroscience. 2012; 222:366–378. [PubMed: 22728101]

Giza CC, Mink RB, Madikians A. Pediatric traumatic brain injury: not just little adults. Curr Opin Crit Care. 2007; 13:143–152. [PubMed: 17327734]

Gonzalez MI, Krizman-Genda E, Robinson MB. Caveolin-1 regulates the delivery and endocytosis of the glutamate transporter, excitatory amino acid carrier 1. J Biol Chem. 2007; 282:29855–29865. [PubMed: 17715130]

Gu Y, Zheng G, Xu M, Li Y, Chen X, Zhu W, Tong Y, Chung SK, Liu KJ, Shen J. Caveolin-1 regulates nitric oxide-mediated matrix metalloproteinases activity and blood-brain barrier permeability in focal cerebral ischemia and reperfusion injury. J Neurochem. 2011

Head BP, Patel HH, Tsutsumi YM, Hu Y, Mejia T, Mora RC, Insel PA, Roth DM, Drummond JC, Patel PM. Caveolin-1 expression is essential for N-methyl-D-aspartate receptor-mediated Src and extracellular signal-regulated kinase 1/2 activation and protection of primary neurons from ischemic cell death. FASEB J. 2008; 22:828–840. [PubMed: 17905724]

Ikezu T, Ueda H, Trapp BD, Nishiyama K, Sha JF, Volonte D, Galbiati F, Byrd AL, Bassell G, Serizawa H, Lane WS, Lisanti MP, Okamoto T. Affinity-purification and characterization of caveolins from the brain: differential expression of caveolin-1, -2, and -3 in brain endothelial and astroglial cell types. Brain Res. 1998; 804:177–192. [PubMed: 9841091]

Jasmin JF, Malhotra S, Singh Dhallu M, Mercier I, Rosenbaum DM, Lisanti MP. Caveolin-1 deficiency increases cerebral ischemic injury. Circulation research. 2007; 100:721–729. [PubMed: 17293479]

Jodoin J, Demeule M, Fenart L, Cecchelli R, Farmer S, Linton KJ, Higgins CF, Beliveau R. P-glycoprotein in blood-brain barrier endothelial cells: interaction and oligomerization with caveolins. J Neurochem. 2003; 87:1010–1023. [PubMed: 14622130]

Komarova Y, Malik AB. Regulation of endothelial permeability via paracellular and transcellular transport pathways. Annu Rev Physiol. 2010; 72:463–493. [PubMed: 20148685]

Lajoie P, Goetz JG, Dennis JW, Nabi IR. Lattices, rafts, and scaffolds: domain regulation of receptor signaling at the plasma membrane. J Cell Biol. 2009; 185:381–385. [PubMed: 19398762]

McCaffrey G, Staatz WD, Quigley CA, Nametz N, Seelbach MJ, Campos CR, Brooks TA, Egleton RD, Davis TP. Tight junctions contain oligomeric protein assembly critical for maintaining blood-brain barrier integrity in vivo. J Neurochem. 2007; 103:2540–2555. [PubMed: 17931362]

McCaffrey G, Staatz WD, Sanchez-Covarrubias L, Finch JD, Demarco K, Laracuente ML, Ronaldson PT, Davis TP. P-glycoprotein trafficking at the blood-brain barrier altered by peripheral inflammatory hyperalgesia. J Neurochem. 2012; 122:962–975. [PubMed: 22716933]

McCaffrey G, Willis CL, Staatz WD, Nametz N, Quigley CA, Hom S, Lochhead JJ, Davis TP. Occludin oligomeric assemblies at tight junctions of the blood-brain barrier are altered by hypoxia and reoxygenation stress. J Neurochem. 2009; 110:58–71. [PubMed: 19457074]

Nag S, Manias JL, Stewart DJ. Expression of endothelial phosphorylated caveolin-1 is increased in brain injury. Neuropathol Appl Neurobiol. 2009; 35:417–426. [PubMed: 19508446]

Nag S, Venugopalan R, Stewart DJ. Increased caveolin-1 expression precedes decreased expression of occludin and claudin-5 during blood-brain barrier breakdown. Acta Neuropathol. 2007; 114:459–469. [PubMed: 17687559]

Pellerin L, Magistretti PJ. Glutamate uptake into astrocytes stimulates aerobic glycolysis: a mechanism coupling neuronal activity to glucose utilization. Proc Natl Acad Sci U S A. 1994; 91:10625–10629. [PubMed: 7938003]

Pop V, Badaut J. A Neurovascular Perspective for Long-Term Changes After Brain Trauma. Translational stroke research. 2011; 2:533–545. [PubMed: 22350620]

Pop V, Sorensen DW, Kamper JE, Ajao DO, Murphy MP, Head E, Hartman RE, Badaut J. Early brain injury alters the blood-brain barrier phenotype in parallel with beta-amyloid and cognitive changes in adulthood. J Cereb Blood Flow Metab. 2013; 33:205–214. [PubMed: 23149553]

Predescu SA, Predescu DN, Malik AB. Molecular determinants of endothelial transcytosis and their role in endothelial permeability. Am J Physiol Lung Cell Mol Physiol. 2007; 293:L823–L842. [PubMed: 17644753]

Razani B, Engelman JA, Wang XB, Schubert W, Zhang XL, Marks CB, Macaluso F, Russell RG, Li M, Pestell RG, Di Vizio D, Hou H Jr, Kneitz B, Lagaud G, Christ GJ, Edelmann W, Lisanti MP.

Caveolin-1 null mice are viable but show evidence of hyperproliferative and vascular abnormalities. J Biol Chem. 2001; 276:38121–38138. [PubMed: 11457855]

Readnower RD, Chavko M, Adeeb S, Conroy MD, Pauly JR, McCarron RM, Sullivan PG. Increase in blood-brain barrier permeability, oxidative stress, and activated microglia in a rat model of blast-induced traumatic brain injury. J Neurosci Res. 2010; 88:3530–3539. [PubMed: 20882564]

Regina A, Jodoin J, Khoueir P, Rolland Y, Berthelet F, Moumdjian R, Fenart L, Cecchelli R, Demeule M, Beliveau R. Down-regulation of caveolin-1 in glioma vasculature: modulation by radiotherapy. J Neurosci Res. 2004; 75:291–299. [PubMed: 14705150]

Schneier AJ, Shields BJ, Hostetler SG, Xiang H, Smith GA. Incidence of pediatric traumatic brain injury and associated hospital resource utilization in the United States. Pediatrics. 2006; 118:483–492. [PubMed: 16882799]

Schubert W, Frank PG, Woodman SE, Hyogo H, Cohen DE, Chow CW, Lisanti MP. Microvascular hyperpermeability in caveolin-1 (−/−) knock-out mice. Treatment with a specific nitric-oxide synthase inhibitor, L-NAME, restores normal microvascular permeability in Cav-1 null mice. J Biol Chem. 2002; 277:40091–40098. [PubMed: 12167625]

Shin T. Increases in the phosphorylated form of caveolin-1 in the spinal cord of rats with clip compression injury. Brain Res. 2007; 1141:228–234. [PubMed: 17275798]

Shin T, Kim H, Jin JK, Moon C, Ahn M, Tanuma N, Matsumoto Y. Expression of caveolin-1, -2, and -3 in the spinal cords of Lewis rats with experimental autoimmune encephalomyelitis. J Neuroimmunol. 2005; 165:11–20. [PubMed: 15925413]

Shlosberg D, Benifla M, Kaufer D, Friedman A. Blood-brain barrier breakdown as a therapeutic target in traumatic brain injury. Nat Rev Neurol. 2010; 6:393–403. [PubMed: 20551947]

Siddiqui MR, Komarova YA, Vogel SM, Gao X, Bonini MG, Rajasingh J, Zhao YY, Brovkovych V, Malik AB. Caveolin-1-eNOS signaling promotes p190RhoGAP-A nitration and endothelial permeability. J Cell Biol. 2011; 193:841–850. [PubMed: 21624953]

Stamatovic SM, Keep RF, Wang MM, Jankovic I, Andjelkovic AV. Caveolae-mediated internalization of occludin and claudin-5 during CCL2-induced tight junction remodeling in brain endothelial cells. J Biol Chem. 2009; 284:19053–19066. [PubMed: 19423710]

Virgintino D, Robertson D, Errede M, Benagiano V, Tauer U, Roncali L, Bertossi M. Expression of caveolin-1 in human brain microvessels. Neuroscience. 2002; 115:145–152. [PubMed: 12401329]

Wiencken AE, Casagrande VA. Endothelial nitric oxide synthetase (eNOS) in astrocytes: another source of nitric oxide in neocortex. Glia. 1999; 26:280–290. [PubMed: 10383047]

Zschocke J, Bayatti N, Behl C. Caveolin and GLT-1 gene expression is reciprocally regulated in primary astrocytes: association of GLT-1 with non-caveolar lipid rafts. Glia. 2005; 49:275–287. [PubMed: 15494979]

Highlights

1. Phenotypic changes of the blood-brain barrier after Juvenile TBI
2. Endothelial and astrocyte expression of caveolins after juvenile TBI
3. Role of caveolins in cerebrovascular dysfunctions after juvenile TBI
4. Relationship between changes of expression of caveolins and eNOS and proteins of the BBB

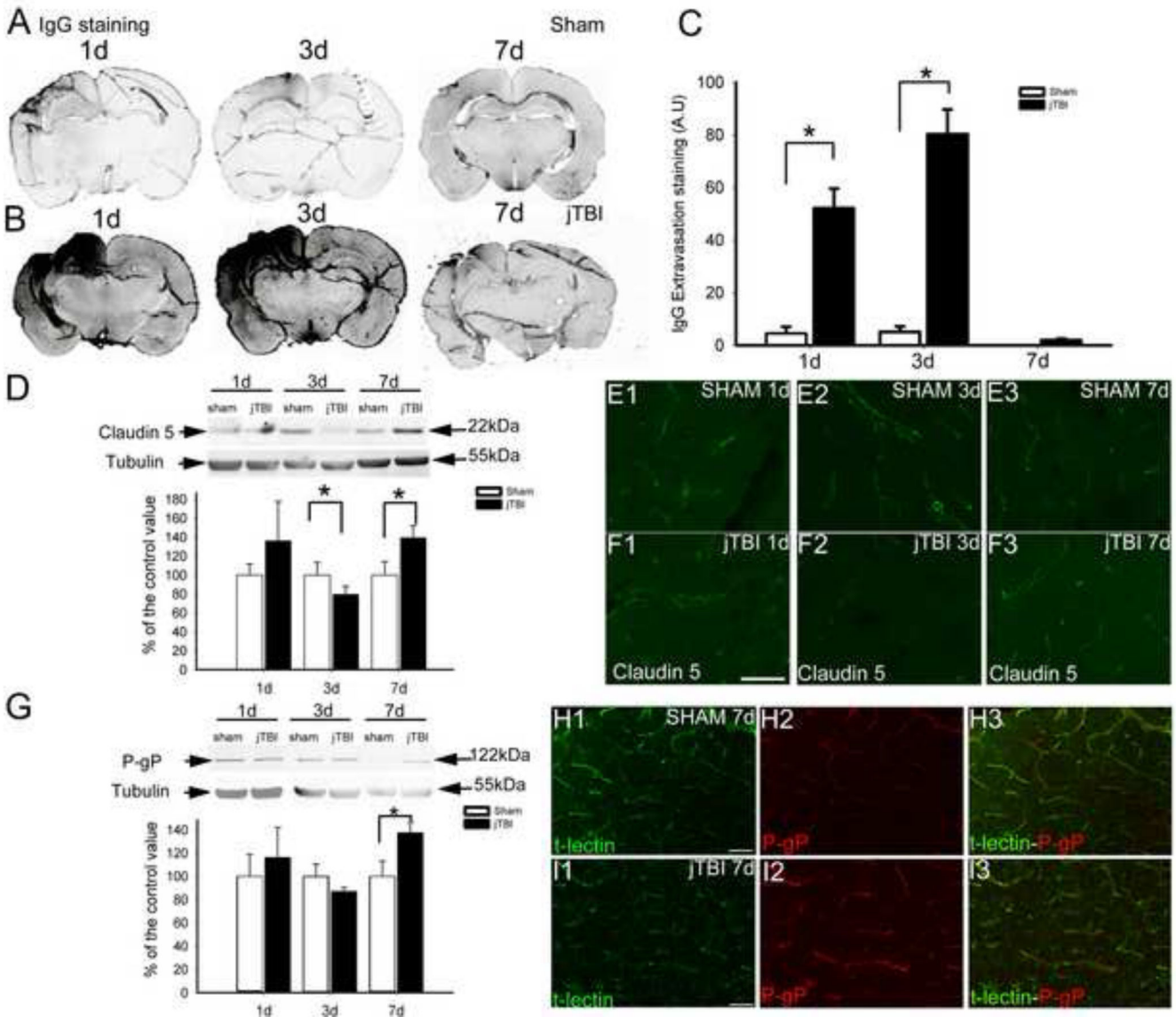

Figure 1. BBB disruption after jTBI

(**A, B**) IgG extravasation staining in sham (A) and jTBI (B) at 1, 3, and 7d post injury. Area of IgG staining (black) is enlarged at 1 and 3d in jTBI animals (B) compared to sham (A), but normalizes by 7d (A, B).

(**C**) Quantification of IgG immunoreactivity shows a significant increase at 1 and 3d, but not at 7d (E; $p<0.05$).

(**D**) Western blot of claudin-5 showed a band around 22kDa and is significantly decreased in jTBI compared to sham at 3 and increased 7d. The quantification of the intensity of the band for claudin-5 was normalized to the tubulin (55kDa).

(**E, F**) A tight junction protein Claudin-5 staining in the sham (E) and jTBI (F) at 1d (E1, F1), 3d (E2, F2) and 7d (E3, F3). Accordingly to western blot (D), the staining of claudin-5 is lower in jTBI (E2) than sham group (F2) at 1d and 3d. Intensity of claudin-5 staining in jTBI group is increased at 7d after the injury (E3, F3).

(**G**) Western blot of P-gp showed a band around 122kDa and is significantly increased in jTBI compared to sham at 7d. The quantification of the intensity of the band for P-gp was normalized to the tubulin (55kDa).

(**H, I**) Tomato-lectin (t-lectin, green, H1, I1) was co-stained with P-gp immunolabeling (red, H2, I2) in the sham (H) and and jTBI (I) at 7d. Accordingly to western blot (G), the staining of P-gp is increased in intensity (red) in blood vessels (outlined by t-lectin, green) in jTBI animals compared to shams.

E, F, H, I bar = 100μm

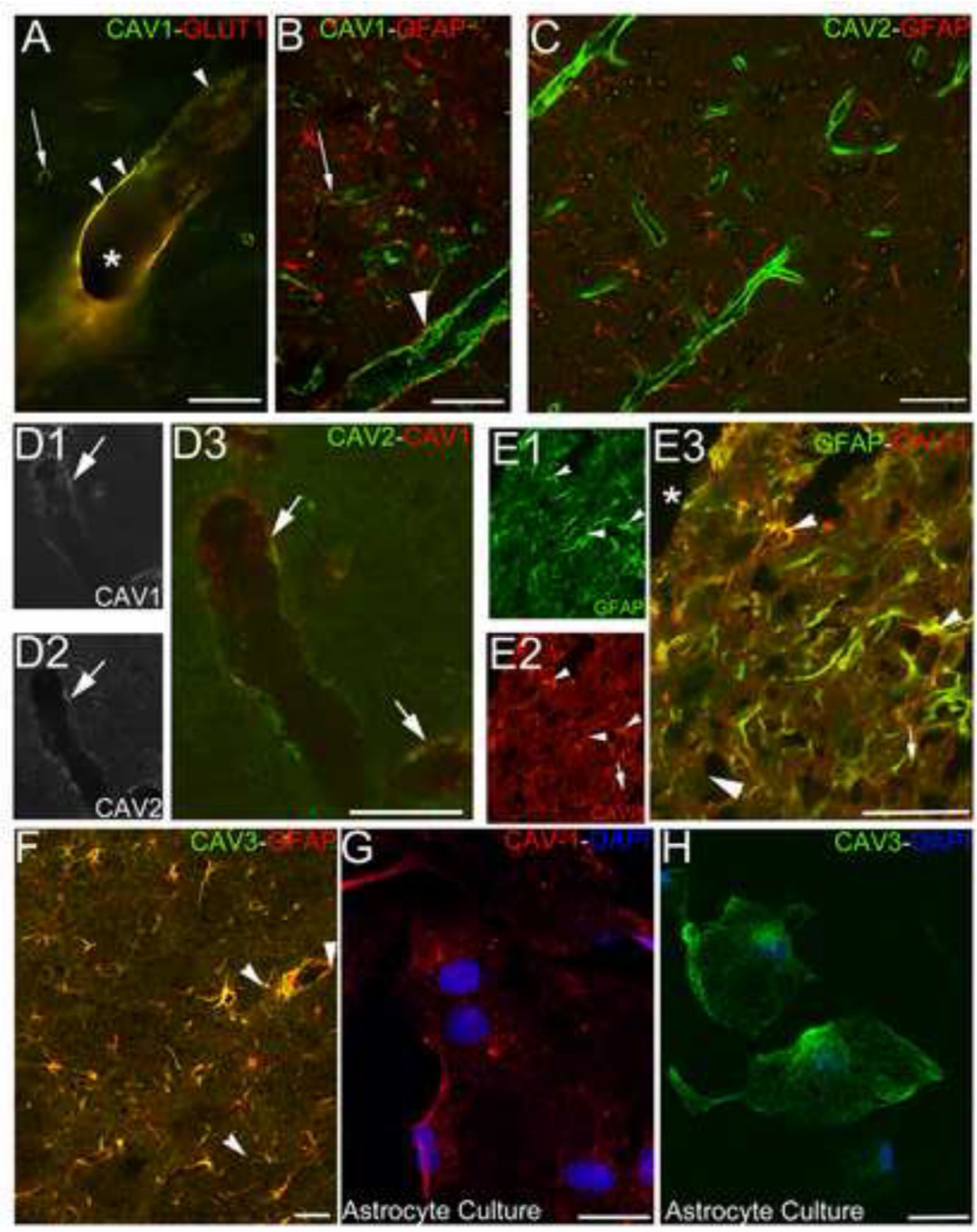

Figure 2. Caveolin distribution in vascular endothelium and astrocytes

(**A**) Mouse anti-cav1 (green) exhibit a staining in the cerebral blood vessels (asterisk), from the large blood vessels to capillary bed (arrows). Co-staining cav-1 (green) and anti-GLUT1, marker for the endothelial cells, shows a co-localization in yellow (arrow heads) in large blood vessels as well as in capillaries.

(**B**) The co-staining cav-1 (green) and anti-GFAP (red) did not show overlap in parietal cortex at distance to the injury site, astrocytic cav-1 staining may be contained within

reactive astrogliosis around the injury (arrowhead = astrocyte endfeet, arrow = cav1 in endothelium).

(**C**) Caveolin-2 (cav-2, green) and GFAP (red) did not exhibit co-localization, only endothelial staining was observed.

(**D**) Double immunolabeling cav-2 (C1, green C3) and cav-1 (C2, red C3) showed co-localization between both staining in the endothelial cells (arrows).

(**E**) In the perilesional areas, rabbit anti-cav-1 staining (red, C2, C3) was co-localized with GFAP labeling (green, C1, C3) (arrowheads), which is an astrocytic marker and increased in reactive astrogliosis.

(**F**) Cav-3 staining (red) and GFAP labeling (green) showed co-localization (yellow, arrowheads), showing the presence of cav-3 in astrocyte process and cell bodies.

(**G**) Cav-1 labeling (red) and nuclear staining with DAPI (blue) in primary astrocyte culture shows presence of cav-1 in the astrocytes.

(**H**) Cav-3 labeling (green) and nuclear staining DAPI (blue) in primary astrocyte culture show the presence of cav-3 protein in the astrocyte.

A = 50μm B, C, D, E, bar = 100μm; F, G, bar=10μm

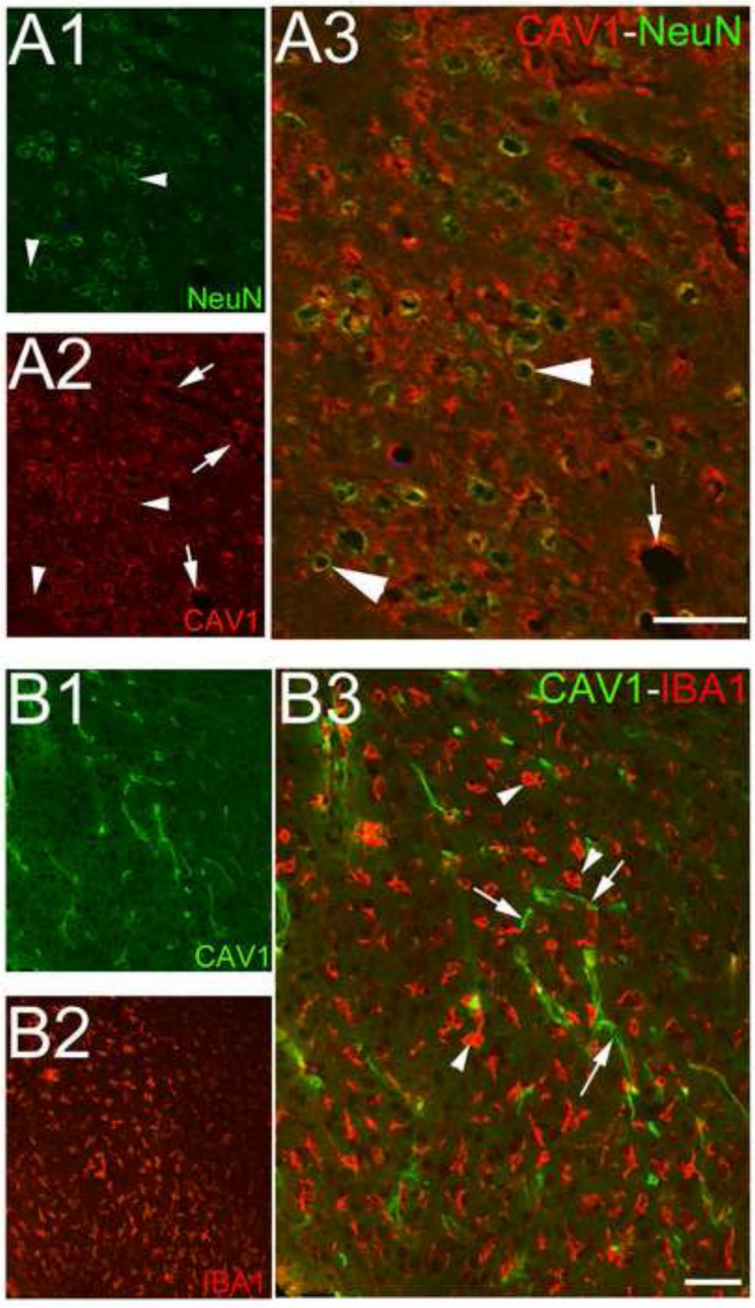

Figure 3. Caveolin 1 expression in neurons but not microglial cells after jTBI

(A) NeuN labeling (green, A1, A3) and Cav-1 staining (red, A2, A3) co-localized (yellow, arrowheads), suggesting the presence of cav-1 in neurons in the periphery of the lesion. Cav-1 staining (red, A2, A3) is also observed in intracortical microvessels (arrows).

(B) Cav-1 labeling (green, B1, B3, arrows) and IBA1 staining (red, B2, B3, arrowhead), a marker of microglial cells, did not show co-localization.

A, bar = 500μm; B, bar = 100μm

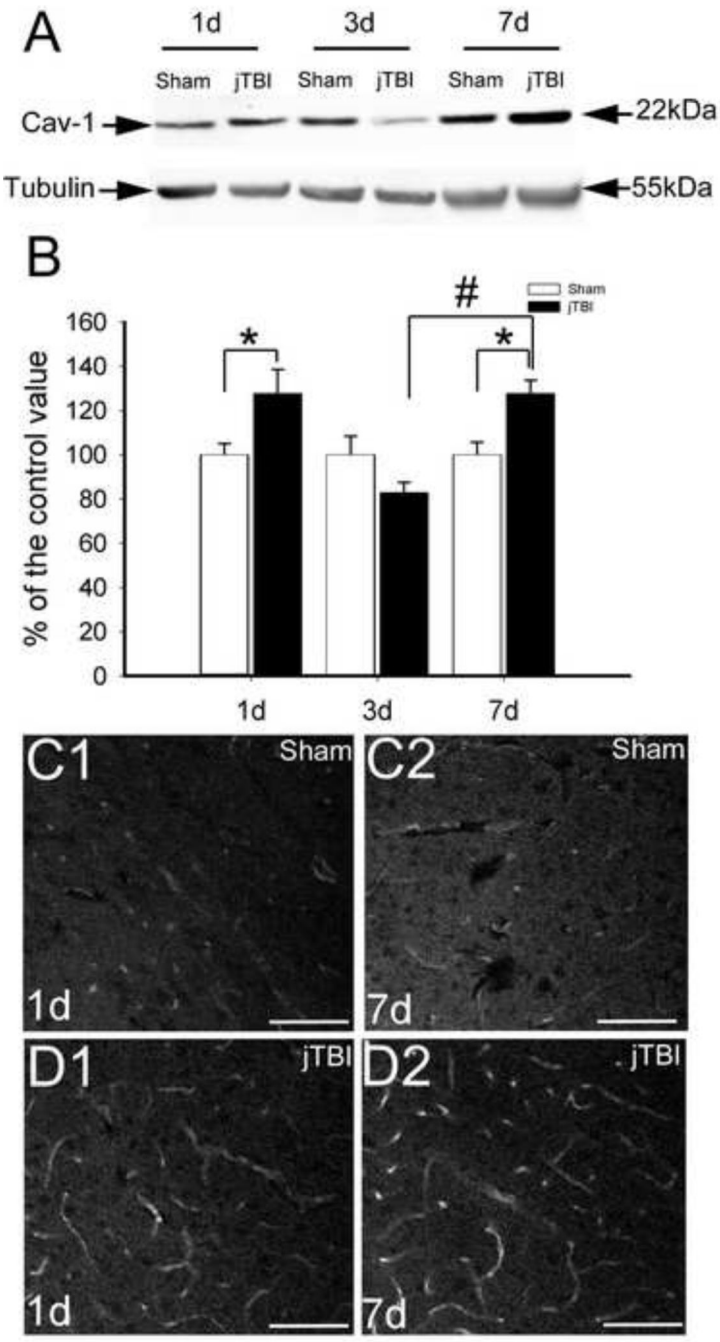

Figure 4. Caveolin 1 Expression after jTBI

(**A**) Western blot for cav-1 showed monomer at 22 kDa and tubulin at 55kDa in sham and jTBI ipsilateral cortex. Cav-1 is increased at 1d and 7d in jTBI animal compared to shams. In contrast at 3d, the intensity of the band for cav-1 is lower in jTBI group than sham

(**C**) Quantification of cav-1 from western blots showed significant increases in jTBI animals compared to sham at 1d and 7d (*, $p<0.05$). The increase is significantly higher at 7d than at 3d in jTBI animals (#, $p<0.05$).

(**C, D**) Caveolin-1 (cav-1) staining in the sham (C) and jTBI (D) at 1d (C1, D1) and 7d (C2, B2) after the injury. Less endothelial cav-1 staining was observed throughout the time-points studied in sham (A) compared to jTBI (B).
C, D, bar = 100μm

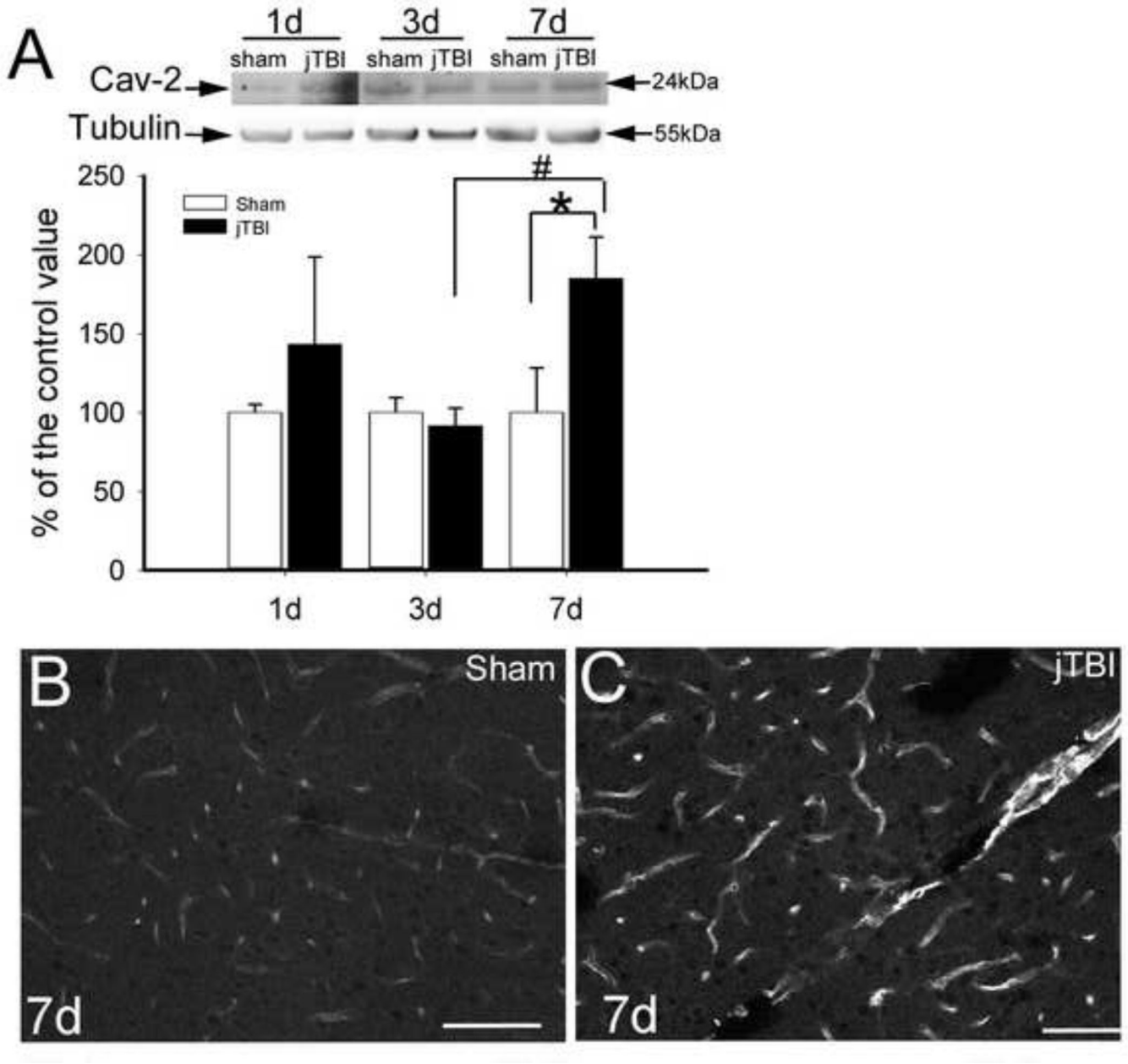

Figure 5. Caveolin 2 Expression expression after jTBI

(**A**) Western blot of cav-2 showed a band around 20kDa with a significant increase in intensity between sham and jTBI group at 7d post-injury (*$p<0.05$). In jTBI group, cav-2 is significantly increase between 3 and 7d (#, $p<0.05$)

(**B**, **C**) Cav-2 staining in the sham (C) and jTBI (D) at 7d exhibits higher intensity of staining in cortical blood vessels of the jTBI group than in sham

B, C, bar = 100μm

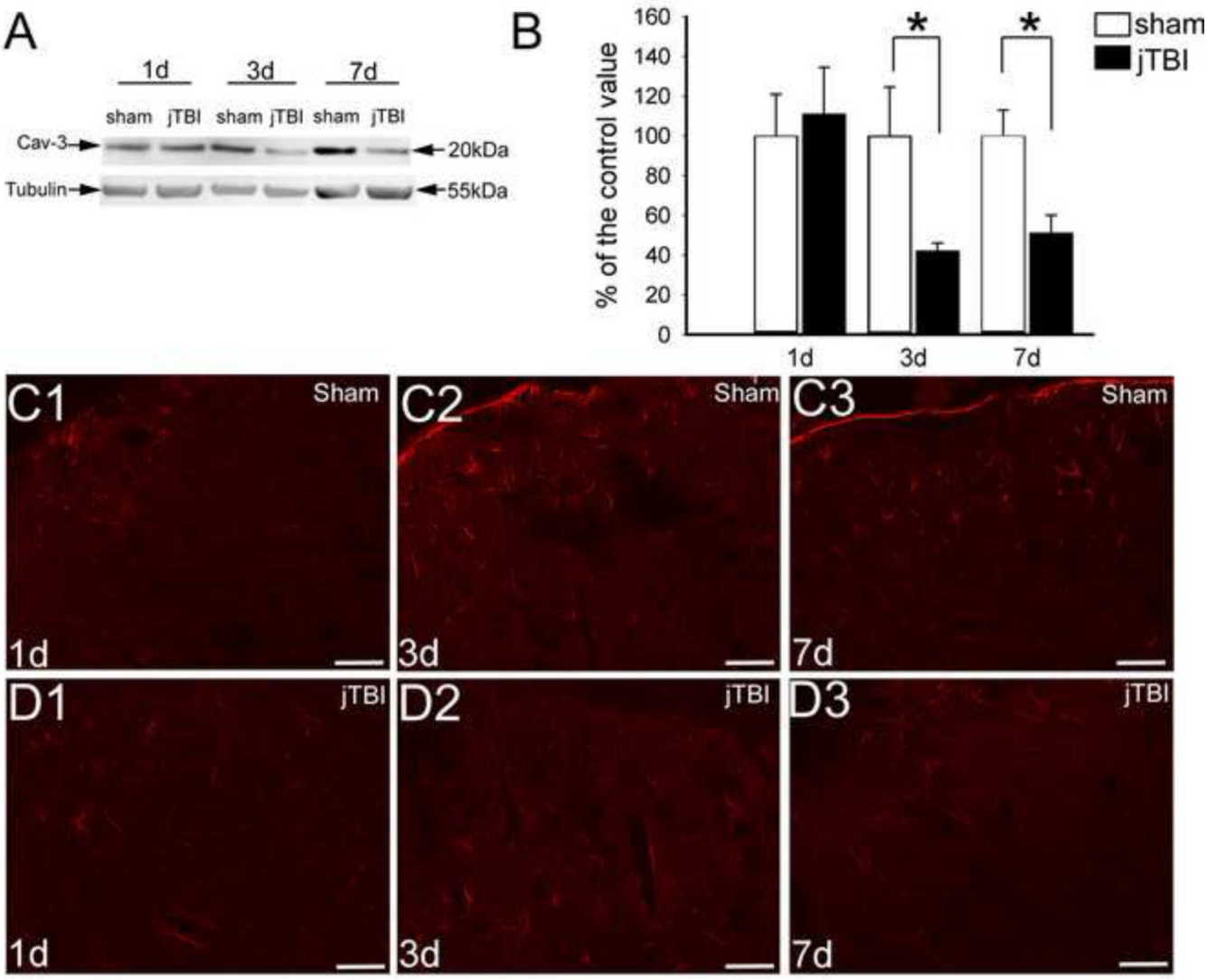

Figure 6. Caveolin-3 Expression and Distribution after jTBI

(**A**) Western blot of cav-3 (red) showed a band around 20kDa and is significantly decreased in jTBI compared to sham at 3 and 7d.

(**B**) The quantification of the intensity of the band for cav-3 was normalized to the tubulin (55kDa).

(**C**, **D**) Cav-3 staining in the sham (C) and jTBI (D) at 1d (C1, D1), 3d (C2, D2) and 7d (C3, D3). In accordance with the western blot, no major changes were observed in cav-3 staining at 1d (C1, D1). However, the pattern of cav-3 staining differs between the jTBI and sham animals at 3d (C2, D2) and 7d (C3, D3). In the glia limitans, cav-3 staining is decreased in jTBI animals (D2, D3) compared to sham (C2, C3). The intensity of cav-3 staining is decreased in jTBI animals (D2, D3) compared to sham (D2, D3) despite an increase of the extend of the surface staining for cav-3 in jTBI group at both time points.

C, D, bar = 100μm

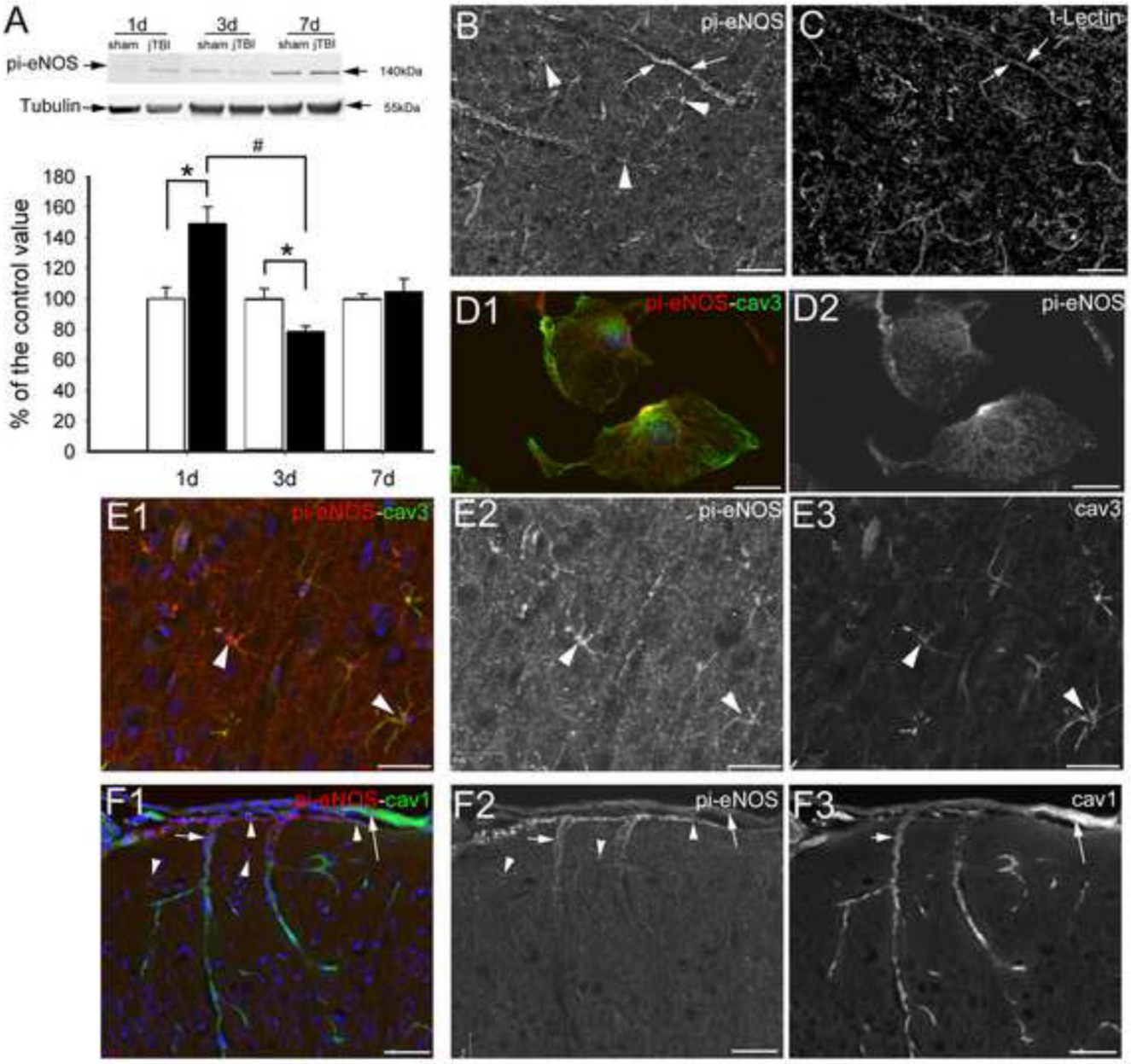

Figure 7. pi-eNOS expression and distribution after jTBI

(**A**) Western blot of pi-eNOS showed a band around 140kDa and is significantly increased in jTBI compared to sham at 1d (*, $p < 0.05$) and decreased at 3d (*, $p<0.05$). The quantification of the intensity of the band for claudin-5 was normalized to the tubulin (55kDa).

(B, C) The anti pi-eNOS staining (B, arrows) is present in the blood vessels revealed by tomato-lectin staining (t-lectin, C, arrows), but also in the astrocytes (arrowheads) in perilesional cortex of jTBI animals.

(**D**). Double immunolabeling cav-3 (green, D1) and pi-eNOS immunolabeling (red, D1, D2) showed a co-localization in primary astrocyte cultures.

(**E**) Double immunolabeling cav-3 (green, E1, E3) and pi-eNOS immunolabeling (red, E1, E2) showed a co-localization in astrocyte like cells (arrowheads) in the cortex of jTBI rats. (**F**) Double immunolabeling cav-1 (green, F1, F3) and pi-eNOS immunolabeling (red, F1, F2) showed a co-localization in endothelial cells (arrows) in the cortex and the pial blood vessels in jTBI rats. In the glia limitans, pi-eNOS staining was observed in the astrocytes of the glia limitans (arrowheads).

B, C, E, F bar = 50μm; D bar = 25μm